

An Original “Click and Bind” Approach for Immobilizing Copper Hexacyanoferrate Nanoparticles on Mesoporous Silica

Raphaël Turgis,[†] Guilhem Arrachart,^{*,†} Carole Delchet,[†] Cyrielle Rey,[†] Yves Barré,[‡] Stéphane Pellet-Rostaing,[†] Yannick Guari,[§] Joulia Larionova,[§] and Agnès Grandjean^{*,†}

[†]Institut de Chimie Séparative de Marcoule, ICSM, UMR 5257 CEA-CNRS-UM2-ENSCM, BP 17171, 30207 Bagnols sur Cèze, France

[‡]CEA/DEN/DTCD/SPDE/Laboratoire Procédés Supercritiques et de Décontamination, BP 17171, Bagnols sur Cèze, France

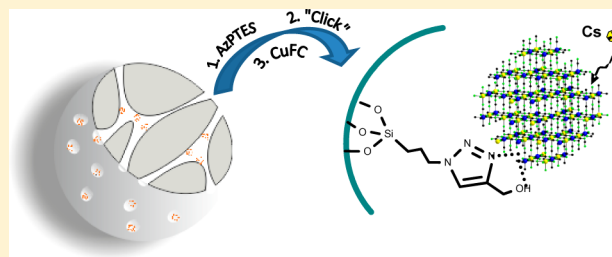
[§]Institut Charles Gerhardt Montpellier, ICGM, UMR 5253 CNRS-UM2-ENSCM-UM1, Chimie Moléculaire et Organisation du Solide, Université Montpellier II, Place E. Bataillon, 34095 Montpellier Cedex 5, France

S Supporting Information

ABSTRACT: We present an original approach for preparing silica-based nanocomposites containing Prussian blue-type nanoparticles via click chemistry. Click reaction is used to prepare a triazole-copper complex in a single step; this complex is subsequently used to anchor copper hexacyanoferrate nanoparticles within a porous silica matrix (porous glass pearls or SBA-15). This CuAAC “click reaction” was performed using a relatively large copper concentration for two reasons: First, the Cu catalyzes the triazole ring formation, then the ring acts as a chelator, immobilizing the copper inside the silica matrix.

Successively adding hexacyanoferrate precursors that coordinate with the copper ions at the triazole sites led to efficient and selective nanocomposite formation; this material was developed to mitigate Cs⁺ ion contamination. The efficiency of these as-prepared nanocomposites and their selectivity for Cs⁺ from different effluents, such as pure water, seawater, and radioactive seawater (simulating the Fukushima site), were evaluated using sorption experiments. These immobilized nanocomposites present a high Cs⁺ selectivity while demonstrating a K_d value above that of the bulk material.

KEYWORDS: click chemistry, mesoporous nanocomposites, copper hexacyanoferrate nanoparticles, cesium decontamination, sorption



1. INTRODUCTION

“Click chemistry” was developed by Sharpless et al. in 2001¹ and is a modular, efficient, and selective route toward high-yield syntheses with little byproduct generation. Intense research has extended click chemistry to include well-known processes, such as the thiol–ene reaction (the addition of an S–H bond across a double bond), oximation (the conversion reaction into an oxime), and Diels–Alder-type reactions (C–C bond formation or cycloaddition). Copper-catalyzed azide–alkyne cycloaddition (CuAAC) (proposed independently by Meldal² and Sharpless³) is among the most developed members of this group. The CuAAC reaction is a powerful tool for covalently binding two appropriate organic molecules to create 1,4-disubstituted 1,2,3-triazoles. This approach has promising applications in various fields, such as drug discovery, dendrimer synthesis, surface modification,⁴ and polymer science.⁵ More recently, CuAAC has been used to functionalize mesostructured silica, offering a simple method for introducing numerous organic functionalities onto/inside hybrid silica pores to generate hybrid materials.⁶ Moreover, “click” reactions have also been used to immobilize metal complexes inside silica pores.⁷ However, despite the ligand-forming ability of CuAAC, reports of porous materials functionalized using 1,2,3-triazole-

based metal complexes are surprisingly scarce. To the best of our knowledge, only one study has reported the synthesis of a grafted triazole-pyridine Pd complex on silica and its use in catalysis.⁸ However, this approach has never been used for anchoring transition metal complexes inside the pores of mesostructured silica or silica-based materials in the aim to preparing nanocomposites based on Prussian blue-type nanoparticles employed for decontamination applications.

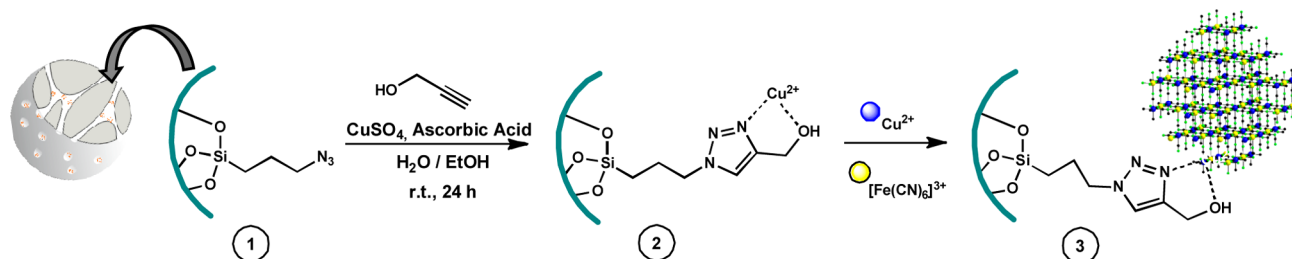
Cyano-bridged coordination polymers $K_xM_y[Fe(CN)_6]_z$ (where M = bivalent transition metal ions) also called Prussian blue analogues (PBAs) are among the best inorganic ionic exchange materials for selective removing radioactive cesium ion from contaminated water, including saline solutions, over a wide pH range.⁹ These materials can selectively remove cesium ions from solution via insertion into the tetrahedral sites of the three-dimensional cyanometallates and/or via monovalent cationic exchange.¹⁰ Because of the high surface-to-volume atomic ratio, nanoscale PBAs exhibit a higher sorption capacity than their bulk counterparts.¹¹ Consequently, several composite materials containing PBA nanoparticles or cyano-bridged

Received: September 6, 2013

Published: October 11, 2013



Scheme 1. Preparation of a Nanocomposite Based on Prussian Blue-type Nanoparticles Inserted into a Silica or Glass Matrix Designed To Extract Cs



bimetallic complexes inside different matrixes have recently been developed. They not only adsorb cesium ions more efficiently but also avoid the drawbacks associated with using PBAs in their bulk form. Most of these composites utilize silica supports and are obtained by successive impregnation of silica with PBAs precipitates^{9c,12} or polymeric layer.¹³ However, the poor reproducibility and inability to control the composition of these materials remain major problems with these approaches. In addition, the PBA particles are weakly linked to the silica support, which could lead to their partial leaching during the cesium extraction process. Therefore, PBA-based dinuclear complexes have been covalently grafted onto sulfide- or ethylene diamine-modified silica to improve the Cs⁺ sorption capacity.^{14,15} In this line of thought, some of us recently reported size-controlled (3–6 nm) cyano-bridged coordination polymeric nanoparticles covalently grafted onto pyridine-modified silica or porous glass.^{11,16,17} These nanocomposites are promising, efficient, and selective Cs⁺ sorbents in pure and saline water allowing for a column decontamination process. However, these materials were designed using ligands that are either expensive or difficult to prepare, hindering the industrialization of this process. In this Article, we report a new, simple synthetic route toward silica- and glass pearl-based nanocomposites using PBA nanoparticles covalently bonded inside the pores for use in Cs⁺ extraction via columns process. The dual-functional click-generated triazole system acts as an immobilizer in the porous matrix and a metal chelator for the Cu²⁺-triazole complex; these structures serve as an anchoring point for forming PBA nanoparticles. Two types of porous silica supports, glass pearls for use in flow experiments and ordered mesoporous silica as a model support, are employed as the matrixes for growing the PBA nanoparticles. The nanocomposites' ability to remove the radioactive cesium from both waste- and seawater is subsequently examined.

2. EXPERIMENTAL SECTION

2.1. Characterization Methods. Solid-state FT-IR spectra were obtained using an ATR crystal or KBr pellets on a Perkin-Elmer 100 spectrometer at 4 cm⁻¹ resolution.

The ¹H, ¹³C, and ²⁹Si NMR spectra were obtained with a Bruker 400 ultrashield VS spectrometer using deuterated chloroform as the solvent and internal standard. The chemical shifts are reported in parts per million (ppm). The ¹³C and ²⁹Si CP MAS NMR spectra were recorded on a Bruker 400 ultrashield VS spectrometer with a 12-kHz MAS spinning rate (the typical contact time was 2–3 ms, and the typical recycle delay was 5–30 s) and Bruker MAS probes (4 mm rotors).

The carbon analysis was performed with a LECO CS-230 carbon/sulfur analyzer. Combustion of the 10-mg samples was carried out under oxygen in an induction oven to create carbon dioxide gas that was analyzed using an infrared solid detector.

Thermal analysis was performed with a Setaram instrument under flowing air heated at 5 °C/min.

Powder X-ray diffraction patterns were obtained with a Bruker D8 advanced diffractometer in a Bragg–Brentano geometry using Ni-filtered Cu K α radiation. The crystallite sizes (*L*) were estimated from the line broadening in the XRD peaks using the Scherrer formula in which λ is the wavelength of the X-rays, β is the full-width at half-maximum height, and θ is the diffraction angle.

$$L = \frac{0.94\lambda}{\beta \cos \theta} \quad (1)$$

Transmission electron microscopy (TEM) was carried out at 200 kV on a JEOL 200CX microscope.

The cesium concentrations were measured using ion chromatography (Dionex). The solutions were injected onto a column with a 30 °C mobile phase. The Cs species were retained on the stationary phase and eluted after 30 min as determined via conductivity.

2.2. Synthesis. Commercially available glass Vycor pearls were the first supports tested and ranged in size from 200 to 500 μ m with 28 nm pores (as determined using the Barrett–Joyner–Halenda (BJH) method) and a 113 m²/g specific surface (as determined using the Brunauer–Emmett–Teller (BET) method). The second support was ordered mesoporous silica SBA, which was synthesized as previously reported.¹⁸ The pore size of 9.4 nm and specific surface of 540 m²/g were determined using the BJH and BET methods, respectively. These results corresponded to a 144 m²/g microporous surface (pore size below 2 nm) and a 396 m²/g mesoporous surface as determined using a t-plot.

The anhydrous solvents were purchased from Acros Organics. The 3-chlorotriethoxypropylsilane, sodium azide, ascorbic acid, copper sulfate, propargyl alcohol, copper(II) tetrafluoroborate, potassium hexacyanoferrate (K₃Fe(CN)₆), and tetrabutylammonium perchlorate [N(C₄H₉)₄]ClO₄ were purchased from Aldrich and used as received; the (N(C₄H₉)₄)₃(Fe(CN)₆) was obtained by reacting K₃Fe(CN)₆ with [N(C₄H₉)₄]ClO₄ in methanol as previously described.¹⁹

The syntheses of the molecular precursor and all other materials were carried out under nitrogen using vacuum-line and Schlenk techniques.

Synthesis of 3-Azidopropyltriethoxysilane (AzPTES). The 3-azidopropyltriethoxysilane was prepared according the literature.^{7a} To a solution of tetrabutylammonium bromide (3.2 g, 10 mmol) and sodium azide (10 g, 154 mmol) in dry acetonitrile (150 mL) was added 3-chloropropyltriethoxysilane (10 mL, 42 mmol). The heterogeneous mixture was then heated to 90 °C under an inert atmosphere for 18 h. The solvent was removed via distillation under reduced pressure, and the residue was washed with pentane.

The mixture was filtered through Celite under argon, and the solvent was removed via distillation under vacuum. The 3-azidopropyltriethoxysilane (AzPTES) was obtained as a colorless oil (6.2 g, 60%).

¹H NMR (CDCl₃): δ (ppm) = 3.75 (q, *J* = 7.0 Hz, 6 H; CH₃CH₂O), 3.20 (t, *J* = 7.0 Hz, 2H; CH₂N₃), 1.64 (m, 2H; SiCH₂CH₂), 1.16 (t, *J* = 7.0 Hz, 9H, CH₃CH₂O), 0.61 (m, 2H; SiCH₂). ¹³C NMR (CDCl₃) δ (ppm): 58.4 (CH₃CH₂O), 53.8 (CH₂N₃), 22.6 (SiCH₂CH₂), 18.2 (CH₃CH₂O), 7.6 (SiCH₂). ²⁹Si

NMR (CDCl₃): δ (ppm) = -46.3. IR (ATR crystal): ν (cm⁻¹) 2095 (-N₃ ν_{as}).

Cu-Triazole Complex Formation Inside Porous Matrixes. The precursor quantities used during the following reactions were determined on the basis of the theoretical amount of silanol at the porous surface (6 silanol per nm²²⁰) linking the specific surface area to the stoichiometry. The AzPTES was present in 1 mol equiv relative to the theoretical quantity of silanol on the surface of the support (estimated at 1.13 and 5.4 mmol/g for the porous glass and SBA-15 matrix, respectively). The synthesis of the azido-functionalized composite (azide-functionalized porous glass pearls (GP-N3) or mesostructured silica (SBA-N3)) occurred after grafting the 3-azidopropyltriethoxysilane onto the glass pearls or porous silica SBA15 (see Scheme 1, step 1).

A mixture of the 3-azidopropyltriethoxysilane (1.02 g) and porous glass (3.7 g) (or 0.77 g of SBA15) in 100 mL of dry toluene was refluxed (115 °C) under an Ar atmosphere for 24 h. After being cooled, the solid product was filtered and washed with ether.

The cycloaddition of the azido-silica with the propargyl alcohol was performed in the presence of ascorbic acid with a copper sulfate catalyst (see Scheme 1, step 2).

A stoichiometric excess of copper instead of the typical catalytic quantity was used during the CuAAC reaction to ensure that the triazole-copper complex formed in the porous material. The azide-functionalized material (GP-N3 or SBA-N3) reacted with 2.5 equiv of propargyl alcohol in a 1:1 water/ethanol mixture containing copper sulfate (2 equiv) and ascorbic acid (5 equiv) in a typical click procedure.

Five grams of GP-N3 (or 1.22 g of SBA-N3) was added to absolute ethanol with 0.125 g of propargyl alcohol. The copper sulfate (0.43 g) and ascorbic acid (0.77 g) were diluted in ultrapure water and subsequently mixed with the azide in 50% aqueous ethanol over 24 h.

The solid product (GP-triazole or SBA-triazole) was filtered and washed thoroughly with ethanol and acetone.

Synthesis of the Nanocomposites. The Cu²⁺/[Fe(CN)₆]³⁻ nanoparticles were grown inside the grafted glass or SBA support as described in the literature²¹ (see Scheme 1, step 3). The GP-triazole or SBA-triazole was treated five times consecutively with a methanolic Cu(TBF₄)₂ solution followed by a methanolic [N(C₄H₉)₄]₃[Fe(CN)₆] solution. At each step, the as-obtained powders were thoroughly washed with methanol. After the fifth step, the solid products (GP-CuFC and SBA-CuFC) were dried overnight in air. The elemental analyses of the nanocomposites are given in Supporting Information Table S1.

2.3. Cesium Sorption Experiments. The Cs sorption experiments were conducted in three different environments: pure water, saline (seawater), and saline with radioactive Cs to simulate the effluents from the Fukushima site. The saline (seawater) solution was analyzed using ICP-MS yielding the following composition: Na (9.6 g/L), Mg (1.28 g/L), Ca (0.4 g/L), K (0.5 g/L), and Sr (0.008 g/L) as chloride salts. Equilibrium studies were performed prior to the isotherm adsorption experiments. The adsorption isotherms were plotted from the data obtained at equilibrium. Each Cs⁺ extraction experiment was performed with a batch solution under shaking at room temperature.

The distribution coefficient (K_d (mL/g)) was calculated using the following eq 2 in which C_i is the initial concentration of the metal ion in solution, C_f is the residual metal ion concentration, and V/M is the solution volume to solid-mass ratio (V = volume of the treated solution and m = mass of the nanocomposite used):

$$K_d = \frac{(C_i - C_f)}{C_f} \left(\frac{V}{m} \right) \quad (2)$$

The cation uptake capacity Q (mmol/g) of the samples was calculated using eq 3:

$$Q = (C_i - C_f) \frac{V}{m} \quad (3)$$

Sorption in Pure Water and Saline. In a typical experiment, 10 mg of the nanocomposite was shaken in 20 mL of a 1 mmol/L CsNO₃ solution in deionized or saline water for 24 h at which, according to the literature, equilibrium was reached.⁸ The liquid phase was filtered through a 0.2- μ m cellulose acetate membrane. The concentration of Cs remaining in the liquid phase was determined using ion chromatography.

Sorption in Radioactive Saline Water. A radioactive solution (1 L) was prepared from seawater and radioactive ¹³⁷Cs. Subsequently, 100 mL of ¹³⁷Cs-enriched seawater (29 kBq/L, corresponding to 6.7 \times 10⁻⁸ mmol/L) was shaken with 50 mg of the nanocomposite pearls for 24 h. Afterward, the solution was filtered and analyzed via gamma spectrometry.

3. RESULTS AND DISCUSSION

3.1. Synthesis of Nanocomposites and Their Chemical, Structural, and Morphological Characteristics. The nanocomposites for a selective cesium ion extraction were prepared using a three-step methodology involving a click chemistry process (Scheme 1): (i) a clickable group (N₃-) was introduced onto porous matrixes by covalently grafting the azide; (ii) the click chemistry reaction inside the porous matrixes formed Cu²⁺-triazole complexes grafted into the pores; and (iii) PBA nanoparticles were grown inside the matrix. This approach was used to prepare two types of nanocomposites using either mesoporous silica SBA 15 or porous glass pearls.

In the first step, azidopropyltriethoxysilane (AzPTES) was chosen as the clickable organosilane^{6a,b,7a} and was used to modify the matrix surfaces. The AzPTES was obtained by displacing the chloride from commercially available 3-chloropropyltriethoxysilane using sodium azide. The azido-functionalized matrix 1 (GP-N3 or SBA-N3) was obtained by condensing AzPTES onto the surface/pores of the silica matrix via refluxing in toluene under argon. The FT-IR spectrum of the azido-modified silica materials exhibited a strong peak at approximately 2100 cm⁻¹, which is characteristic of the azide group's asymmetric stretching vibration (see Supporting Information Figure S1). The presence of N₃ functionality was also confirmed in both materials using ¹³C solid-state NMR, which detected a peak at 52.0 ppm corresponding to CH₂N₃ (see Supporting Information Figure S2).

The azido-modified porous matrixes were then added to the propargyl alcohol through a CuAAC reaction to yield SBA15 silica or porous glass matrix 2 functionalized with Cu²⁺-triazole complexes inside its pores (Scheme 1).

This reaction was monitored via FT-IR (see Supporting Information Figure S1) and solid-state NMR (see Supporting Information Figure S2). The triazole stretch was hidden by the bending vibration of the surface-adsorbed water at 1650 cm⁻¹; however, the click reaction could be followed using the disappearance of the azide stretching vibration at 2100 cm⁻¹ to verify the complete conversion of the N₃ groups into the triazole functionalities. This reaction was also confirmed using the signals at 120 and 150 ppm, which are characteristic of 1,4-disubstituted 1,2,3-triazoles in ¹³C solid-state NMR.²²

The quantity of grafted organic groups (Table 1) was estimated using several techniques including TGA, carbon total, and elemental analysis. The organic loading was approximately 0.09 mmol/g for the glass pearls (GP-triazole) and 0.18 mmol/g for the porous silica (SBA-triazole).

The presence of a Cu²⁺-triazole complex attached within the pores after the click reaction was confirmed by elemental analysis, X-EDS (Supporting Information Figure S4), and EPR spectroscopies (Supporting Information Figure S5). The EPR

Table 1. Composition of the Triazole-Based Material and the Corresponding Nanocomposites

	triazole-based material (matrix 2)	nanocomposite (matrix 3)
	organic loading (mmol/g)	CuFC loading (mmol/g)
glass pearl	0.088	0.005
SBA-15	0.183	0.021

spectrum of the sample GP-triazol obtained after the click reaction is typical for powdered Cu^{2+} axial complexes diluted in hosts. The values of g -factors ($g_{\parallel} = 2.22$ and $g_{\perp} = 2.05$) are in agreement with the previously reported results on the Cu^{2+} triazol complexes.²³

The intrapore growth of the cyano-bridged coordination polymer networks beginning with the triazole complexes was performed using a successive impregnation process adapted from previously described procedures.^{11,21} Typically, the nanoparticles were grown using five consecutive treatments with a methanolic $[\text{N}(\text{C}_4\text{H}_9)_4]_3[\text{Fe}(\text{CN})_6]$ solution followed by a methanolic $\text{Cu}(\text{BF}_4)_2$ solution. The material was washed with methanol between each stage of the treatment. The composition of the nanocomposites was determined from the elemental analysis given in Supporting Information Table S1.

The $\text{Cu}^{2+}/[\text{Fe}(\text{CN})_6]^{3-}$ (CuFC) nanoparticle content was estimated at 4.9% in the glass-based (GP-CuFC) and 21.2% in the silica-based (SBA-CuFC) nanocomposites (Table 1). If the surface available for loading the nanoparticles derives from the mesoporous surface area ($396 \text{ m}^2/\text{g}$ for silica and $113 \text{ m}^2/\text{g}$ for glass), the nanoparticle loadings per m^2 for the two supports are surprisingly similar: approximately 4.5×10^{-4} mmol of $\text{Cu}^{2+}/[\text{Fe}(\text{CN})_6]^{3-}/\text{m}^2$ for the GP-CuFC and 5.2×10^{-4} mmol of $\text{Cu}^{2+}/[\text{Fe}(\text{CN})_6]^{3-}/\text{m}^2$ for the SBA-CuFC samples. Even with a smaller surface area on the porous glass than on the mesostructured SBA-15 silica, the nanoparticle loadings per nm^2 remained close.

The nanoparticle growth was followed via FT-IR by monitoring the CN^- stretching vibration mode. The spectra of the nanocomposites exhibit two closed CN stretching vibrations at 2173 and 2105 cm^{-1} for the GP-CuFC and 2166 and 2108 cm^{-1} for the SBA-CuFC material, corresponding to the vibrations observed for the bulk $\text{Cu}_3[\text{Fe}(\text{CN})_6]_2 \cdot 13\text{H}_2\text{O}$ powder (at 2172 and 2097 cm^{-1}) (see Supporting Information Figure S3). Therefore, the formation of the bridging CN^- ligands confirms the formation of the PBA structure.²⁴ The two bands at 2175 and 2110 cm^{-1} were attributed to the stretching of the CN ligand bridged between the Cu^{2+} and Fe^{3+} in a $\text{Cu}^{2+}-\text{CN}-\text{Fe}^{3+}$ mode and to the linkage isomer with a $\text{Cu}^{2+}-\text{NC}-\text{Fe}^{3+}$ coordination mode, as reported for the parent bulk cyano-bridged coordination polymer.²⁵

Powder X-ray diffraction (XRD) also provided information regarding the grafted cyano-bridged coordination polymer nanoparticles inside the matrixes (Figure 1). As compared to the bulk materials, both nanocomposites exhibited phases similar to those of the bulk $\text{Cu}_3[\text{Fe}(\text{CN})_6]_2 \cdot 13\text{H}_2\text{O}$, revealing the presence of the cyano-bridged coordination complexes in these materials.

Relative to the bulk material, the nanocomposites exhibited an intense reflection at $2\theta = 22^\circ$, which may be attributed to a contribution from the silica. The CuFC particle sizes were calculated to be approximately 9 and 8 nm for the GP-CuFC and SBA-CuFC nanocomposites, respectively, using Scherrer's equation (see eq 1) and the reflections at 17° and 35° .

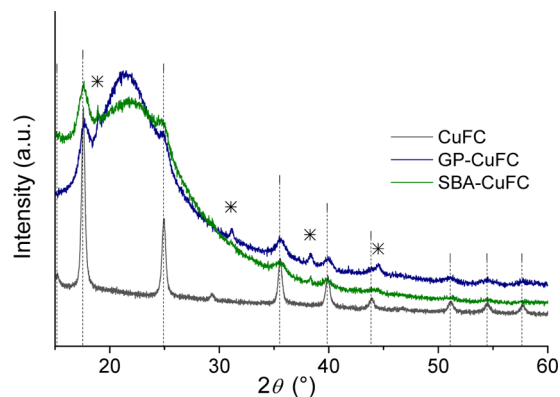


Figure 1. XRD powder data for the CuFC glass pearl and SBA nanocomposites as compared to the bulk $\text{Cu}_3[\text{Fe}(\text{CN})_6]_2 \cdot 13\text{H}_2\text{O}$. Dotted line represents pattern file JCP2.2CA: 01-070-2702 (* K_2SiF_6 impurities, pattern file JCP2.2CA: 00-007-0217).

The textural aspects of the nanocomposites were investigated via scanning (SEM) and transmission electron microscopy (TEM). The SEM observations revealed that the surface characteristics of the pristine matrixes were not altered by the nanoparticle growth. No significant modifications were observed in the glass pearl or silica morphologies except that their color changed from white to brown (Figure 2b). Additionally, no bulk coordination polymer formed outside the matrixes.

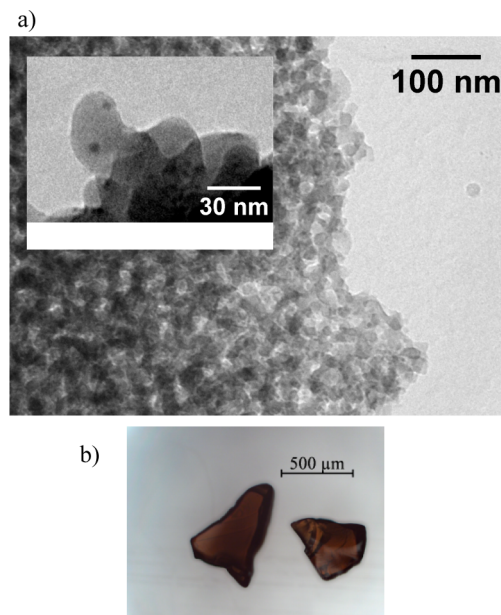


Figure 2. (a) TEM images and (b) an image of the GP-CuFC nanocomposites.

TEM observations confirm the presence of the PBA nanoparticles in the matrix pores. Typical images shown in Figure 2a indicate that the ~ 6 -nm spherical nanoparticles inside the glass pores of the GP-CuFC are consistent with the particle size estimated from the XRD analysis. Similarly, no aggregated bulk cyanometallates were observed outside the glass pores in the TEM images.

Comparing the nitrogen adsorption isotherms of the initial triazole-functionalized materials indicates a decrease in the pore

volume for the PBA nanoparticle-loaded material (Supporting Information Table S2). However, the analysis suggests that no pores in the materials were blocked and the porosity remained accessible (the filled pores are visible in Figure 3). This parameter is critical for materials designed for solid-phase extraction.

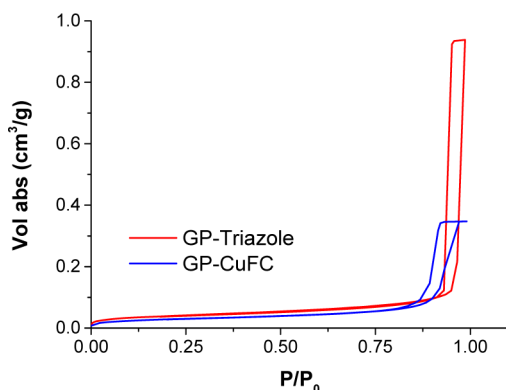


Figure 3. Nitrogen adsorption isotherms for the GP-triazole (red) and the related nanocomposites GP-CuFC (blue).

3.2. Removal of Cs from Contaminated Effluent.

Cesium adsorption experiments were performed to evaluate the adsorption capacity and selectivity of the nanocomposites. Three solutions were used. First, an aqueous solution containing nonradioactive CsCl was used to estimate the maximum adsorption capacity of the nanocomposite. Second, an aqueous saline solution containing nonradioactive CsCl and NaCl was used to determine the nanocomposite's selectivity for cesium. Finally, an aqueous saline solution containing radioactive CsCl (^{137}Cs -enriched seawater at 29 kBq/L, corresponding to 6.7×10^{-8} mmol/L) was used to mimic "real" conditions. A simple static "batch" method was used to characterize the sorption properties of the nanocomposites. The investigated solution and nanocomposites were shaken together for 24 h before separation via filtration.

Several models have been used to describe the extraction of dissolved ions by a solid, all of which are based on the adsorption isotherms that quantify the species (Cs^+) adsorbed onto a solid (Q in mmol/g) versus the concentration of the given species (Cs^+) remaining in solution at equilibrium (C in mmol/L).²⁶ The Langmuir model assumes that adsorption occurs at structurally homogeneous sites and all sorption sites are energetically identical:

$$Q = Q_{\max} + \frac{LC}{1 + LC} \quad (4)$$

in which Q_{\max} is the maximum adsorption capacity that describes the efficiency of the solid for removing cesium ions from solution at or near saturation, and L is the Langmuir constant related to the affinity of the binding sites. The free energy of adsorption (ΔG_L) can be determined using Q_{\max} and L as follows:

$$\Delta G_L = -RT \ln(Q_{\max} L) \quad (5)$$

The isothermal curves for both nanocomposites (GP-CuFC and SBA-CuFC) are compared to that of the bulk (Figure 4) by plotting the quantity of cesium adsorbed per gram of nanoparticles as a function of the quantity of cesium remaining in solution. The Langmuir model fits both nanocomposites

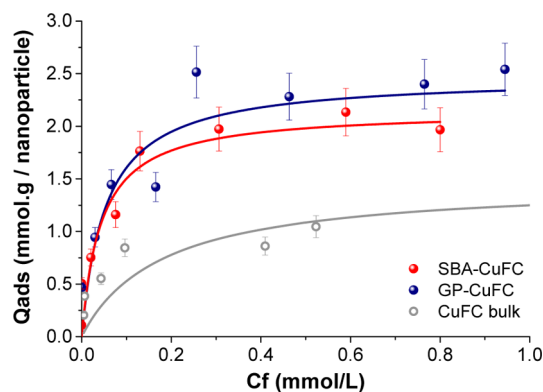


Figure 4. Adsorption isotherms and the Langmuir model for the glass and silica composites containing $\text{Cu}^{2+}/[\text{Fe}(\text{CN})_6]^{3-}$ nanoparticles as compared to bulk $\text{Cu}_3[\text{Fe}(\text{CN})_6]_2 \cdot 13\text{H}_2\text{O}$.

well, confirming an isothermal chemisorption mechanism for both.

The maximum adsorption capacities (Q_{\max}) of nanocomposites obtained using the Langmuir model are 2.47 and 2.17 mmol/g nanoparticle for the silica and glass supports, respectively. The similarity between these values suggests that the nature of the support did not influence the Q_{\max} value. These values are higher than that obtained for the bulk PBA material (1.47 mmol/g).

The free energy of adsorption calculated using the Langmuir model is negative in both cases, confirming that the Cs adsorption is spontaneous and favorable. The obtained values (-9.4 and -9.8 kJ/mol for the GP-CuFC and SBA-CuFC, respectively) are practically equivalent, indicating that the adsorption may be independent of the support.

In addition, the Langmuir free energy of adsorption for these hybrid materials was 2 times lower than that obtained for the bulk materials (-5 kJ/mol).

The distribution coefficient (K_d (mL/g)) is a mass-weighted partition coefficient defined as the equilibrium ratio between the quantities of cesium adsorbed onto the nanocomposite and remaining in solution. The K_d value was determined to evaluate the selectivity of the nanocomposite for cesium when other competitive ions, such as Na^+ , K^+ , and Ca^{2+} , were present.^{26,27}

The distribution coefficient was approximately 10^4 mL/g for both materials and was obtained for both the nonradioactive seawater and the radioactive seawater (Table 2). Therefore, the nanocomposites exhibit a great affinity for Cs^+ ions in contaminated radioactive effluents, even with high sodium concentrations (9.6 g/L). Similar values were obtained for the bulk: $K_d \geq 10^4$ mL/g in seawater.

Table 2. Maximum Adsorption Capacity (Q_{\max}) and the Distribution Coefficient (K_d) for the Nanocomposites and Bulk Material

sorbent	CuFC per nm^2	Q_{\max} (mmol/g of CuFC)	K_d (mL/g) seawater ^a	K_d (mL/g) radioactive seawater ^b
GP-CuFC	0.027	2.47	1.1×10^4	8.4×10^3
SBA-CuFC	0.031	2.15	5.8×10^3	1.9×10^4

^aThe Cs^+ concentration is 0.1 mmol/L (13 ppm). ^bThe Cs^+ concentration is 29 kBq/L (6.7×10^{-8} mmol/L).

Few results involving copper hexacyanoferrate loaded onto inorganic supports have been published. The majority of the published work regards nanocomposites containing PBA included other types of hexacyanoferrate, such as Co or Ni.^{11,27,28} However, the comparison is not relevant in this case because the sorbent differs in nature.

For copper PBA, comparable distribution coefficients (10^4 – 10^3 mL/g) were reported by Milyutin et al.²⁹ for different composite materials (silica-, alumina-, or zirconia-based materials loaded with copper hexacyanoferrate) under comparable conditions ($C_i(^{137}\text{Cs}) = 10 \text{ kBq L}^{-1}$ in alkaline solution simulating the bottom residue from a nuclear power plant using a WWER-type reactor over 48 h with a V/M equal to 2000 mL/g). Similarly, Tsuruoka et al.³⁰ reported a K_d of approximately 5×10^4 mL/g for an adsorbent containing copper ferrocyanides, diatomites, and carbon nanotubes under different adsorption conditions with a much lower initial Cs concentration (1.47 kBq/L). However, the distribution coefficients obtained for our nanocomposites are lower than those of Sangvanish et al.,^{14b} who used self-assembled copper ferrocyanide on a mesoporous silica adsorbent ($K_d \approx 1 \times 10^5$ mL/g), but their result was obtained with a V/M of 2000 mL/g and an initial Cs concentration of 0.5 ppm.

Therefore, as compared to the literature, this work obtained competitive K_d values, even in saline solutions such as seawater. The size of the glass pearl nanocomposites was between 200 and 500 μm , making them an ideal candidate for decontamination in a continuous process, such as in a column or cartridge. Moreover, because the pores of the glass-based nanocomposites close after decontamination, these materials should efficiently confine and store radioactive species.

4. CONCLUSION

In summary, the use of nanocomposites containing PBA nanoparticles covalently linked to a silica-based matrix provides a promising method for cesium ions decontamination. We proposed a simple methodology to obtain such a nanocomposite via click chemistry by immobilizing a copper-triazole complex covalently grafted inside the pores of a silica or glass matrix. This complex was used as an anchoring point for growing the $\text{Cu}^{2+}/[\text{Fe}(\text{CN})_6]^{3-}$ nanoparticles. The silica-based nanocomposites were used as a model to understand the nanoparticle growth mechanism and the Cs^+ sorption, while the glass-based nanocomposites were utilized for an efficient and selective column decontamination of radioactive cesium.

The sorption experiments for the Cs^+ extraction were carried out using different effluents such as pure water, seawater, and simulated radioactive seawater from the Fukushima site. The batch data revealed promising K_d results for the nanocomposites, which were close to those obtained from the bulk PBA. The nanocomposite glass pearls were also designed for insertion into cartridges to decrease the waste produced and increase the efficiency. The experiments carried out with the ^{137}Cs -enriched seawater demonstrated the potential for using these nanocomposite materials in efficient column decontamination processes.

In addition, the nanocomposite glass pearls containing radioactive cesium may act as a confinement matrix because the pores close after extraction.

■ ASSOCIATED CONTENT

Supporting Information

FT-IR spectra of the azido- and triazole-based materials (Figure S1); ^{13}C solid-state NMR of the azido and triazole materials (Figure S2); FT-IR of the SBA-CuFC and GP-CuFC nanocomposites (Figure S3) and X-EDS analysis for the PG-triazole and PG-CuFC (Figure S4); EPR analysis for the PG-triazole (Figure S5); composition of the materials as determined by elemental analysis (Table S1); and nitrogen adsorption results (Table S2). This material is available free of charge via the Internet at <http://pubs.acs.org>.

■ AUTHOR INFORMATION

Corresponding Authors

*Tel.: +33 4 66 79 15 68. Fax: +33 4 66 79 76 11. E-mail: guilhem.arrachart@cea.fr.

*Tel.: +33 4 66 79 66 22. Fax: +33 4 66 79 76 11. E-mail: agnes.grandjean@cea.fr.

Notes

The authors declare no competing financial interest.

■ ACKNOWLEDGMENTS

This work was supported by the University of Montpellier II, the Matinex and the Paris National Research Groups, the CEA, and the CNRS. We thank Johann Ravaut for assistance with the SEM experiments, Henry-Pierre Brau for assistance with the TEM experiments, Bruno Corso for assistance with the XRD experiments, and Guillaume Serve and Célia Lepeyre for their assistance with the radioactive experiments.

■ REFERENCES

- (1) Kolb, H. C.; Finn, M. G.; Sharpless, K. B. *Angew. Chem., Int. Ed.* **2001**, *40*, 2004–2021.
- (2) Tornøe, C. W.; Christensen, C.; Meldal, M. *J. Org. Chem.* **2002**, *67*, 3057–3064.
- (3) Rostovtsev, V. V.; Green, L. G.; Fokin, V. V.; Sharpless, K. B. *Angew. Chem., Int. Ed.* **2002**, *41*, 2596–2599.
- (4) Meldal, M.; Tornøe, C. W. *Chem. Rev.* **2008**, *108*, 2952–3015.
- (5) (a) Kappe, C. O.; Van der Eycken, E. *Chem. Soc. Rev.* **2010**, *39*, 1280–1290. (b) Moses, J. E.; Moorhouse, A. D. *Chem. Soc. Rev.* **2007**, *36*, 1249–1262. (c) Angell, Y. L.; Burgess, K. *Chem. Soc. Rev.* **2007**, *36*, 1674–1689. (d) Qin, A.; Lam, J. W. Y.; Tang, B. Z. *Chem. Soc. Rev.* **2010**, *39*, 2522–2544.
- (6) (a) Guo, Z.; Lei, A.; Liang, X.; Xu, Q. *Chem. Commun.* **2006**, *43*, 4512–4514. (b) Malvi, B.; Sarkar, B. R.; Pati, D.; Mathew, R.; Ajithkumar, T. G.; Sen Gupta, S. *J. Mater. Chem.* **2009**, *19*, 1409–1416. (c) Moitra, N.; Trems, P.; Raehm, L.; Durand, J.-O.; Cattoen, X.; Wong Chi Man, M. *J. Mater. Chem.* **2011**, *21*, 13476–13482.
- (7) (a) Nakazawa, J.; Stack, T. D. P. *J. Am. Chem. Soc.* **2008**, *130*, 14360–14361. (b) Rana, B. S.; Jain, S. L.; Singh, B.; Bhaumik, A.; Sain, B.; Sinha, A. K. *Dalton Trans.* **2010**, *39*, 7760–7767.
- (8) Zhang, G.; Wang, Y.; Wen, X.; Ding, C.; Li, Y. *Chem. Commun.* **2012**, *48*, 2979–2981.
- (9) (a) Haas, P. A. *Sep. Sci. Technol.* **1993**, *28*, 2479–2506. (b) Lehto, J.; Szirtes, L. *Radiat. Phys. Chem.* **1994**, *43*, 261–264. (c) Mimura, H.; Kimura, M.; Akiba, K.; Onodera, Y. *Solvent Extr. Ion Exch.* **1999**, *17*, 403–417.
- (10) (a) Ayrault, S.; Jimenez, B.; Garnier, E.; Fedoroff, M.; J. Jones, D.; Loos-Neskovic, C. *J. Solid State Chem.* **1998**, *141*, 475–485. (b) Loos-Neskovic, C.; Ayrault, S.; Badillo, V.; Jimenez, B.; Garnier, E.; Fedoroff, M.; Jones, D. J.; Merinov, B. *J. Solid State Chem.* **2004**, *177*, 1817–1828. (c) Avramenko, V.; Bratskaya, S.; Zheleznov, V.; Sheveleva, I.; Voitenko, O.; Sergienko, V. *J. Hazard. Mater.* **2011**, *186*, 1343–1350.

- (11) Delchet, C.; Tokarev, A.; Dumail, X.; Toquer, G.; Barré, Y.; Guari, Y.; Guerin, C.; Larionova, J.; Grandjean, A. *RSC Adv.* **2012**, *2*, 5707–5716.
- (12) Mardan, A.; Ajaz, R.; Mehmood, A.; Raza, S. M.; Ghaffar, A. *Sep. Purif. Technol.* **1999**, *16*, 147–158.
- (13) Loos-Neskovic, C.; Vidal-Madjar, C.; Jimenez, B.; Pantazaki, A.; Federici, V.; Tamburini, A.; Fedoroff, M.; Persidou, E. *Radiochim. Acta* **1999**, *85*, 143–148.
- (14) (a) Lin, Y.; Fryxell, G. E.; Wu, H.; Engelhard, M. *Environ. Sci. Technol.* **2001**, *35*, 3962–3966. (b) Sangvanich, T.; Sukwarotwat, V.; Wiacek, R. J.; Grudzien, R. M.; Fryxell, G. E.; Addleman, R. S.; Timchalk, C.; Yantasee, W. *J. Hazard. Mater.* **2010**, *182*, 225–231. (c) Liu, C.; Huang, Y.; Naismith, N.; Economy, J.; Talbott, J. *Environ. Sci. Technol.* **2003**, *37*, 4261–4268.
- (15) Guo, Y.; Guadalupe, A. R.; Resto, O.; Fonseca, L. F.; Weisz, S. *Z. Chem. Mater.* **1999**, *11*, 135–140.
- (16) (a) Clavel, G.; Guari, Y.; Larionova, J.; Guerin, C. *New J. Chem.* **2005**, *29*, 275–279. (b) Folch, B.; Guari, Y.; Larionova, J.; Luna, C.; Sangregorio, C.; Innocenti, C.; Caneschi, A.; Guerin, C. *New J. Chem.* **2008**, *32*, 273–282.
- (17) Grandjean, A.; Barré, Y.; Guari, Y.; Larionova, J.; Guerin, C. Patents FR2945756 A1 20101126 and WO 2010 133689 A2 20101125, 2010.
- (18) Zhao, D. Y.; Huo, Q. S.; Feng, J. L.; Chmelka, B. F.; Stucky, G. *D. J. Am. Chem. Soc.* **1998**, *120*, 6024–6036.
- (19) Noffle, R. E.; Pletcher, D. *J. Electroanal. Chem.* **1990**, *293*, 273–277.
- (20) Zhuravlev, L. T. *Colloids Surf, A* **2000**, *173*, 1–38.
- (21) Folch, B.; Guari, Y.; Larionova, J.; Luna, C.; Sangregorio, C.; Innocenti, C.; Caneschi, A.; Guerin, C. *New J. Chem.* **2008**, *32*, 273–282.
- (22) Rodios, N. A. *J. Heterocycl. Chem.* **1984**, *21*, 1169–1173. Hoffmann, B.; Bernet, B.; Vasella, A. *Helv. Chim. Acta* **2002**, *85*, 265–287.
- (23) (a) Lever, A. B. P. *Inorganic Electronic Spectroscopy*, 2nd ed.; Elsevier: Amsterdam, 1984; pp 554–572. (b) Mabbs, F. E.; Collison, D. *Electron Paramagnetic Resonance of d Transition Metal Compounds*; Elsevier: Amsterdam, 1992; p 20. (c) Butsch, K.; Klein, A.; Nitsche, S.; Stirnat, K.; Hawkett, J. R.; McInnes, E. J. L.; Bauer, M. *Dalton Trans.* **2012**, *41*, 11464–11475.
- (24) Bertran, J. F.; Pascual, J. B.; Hernandez, M.; Rodriguez, R. *React. Solids* **1988**, *5*, 95–100.
- (25) (a) Reguera, E.; Bertran, J. F.; Diaz, C.; Blanco, J.; Rondon, S. *Hyperfine Interact.* **1990**, *53*, 391–395. (b) Buchold, D. H. M.; Feldmann, C. *Chem. Mater.* **2007**, *19*, 3376–3380.
- (26) Crini, G.; Peindy, H. N.; Gimbert, F.; Robert, C. *Sep. Purif. Technol.* **2007**, *53*, 97–110.
- (27) Lin, Y. H.; Fryxell, G. E.; Wu, H.; Engelhard, M. *Environ. Sci. Technol.* **2001**, *35*, 3962–3966.
- (28) Chang, C.-Y.; Chau, L.-K.; Hu, W.-P.; Wang, C.-Y.; Liao, J.-H. *Microporous Mesoporous Mater.* **2008**, *109*, 505–512.
- (29) Milyutin, V. V.; Mikheev, S. V.; Gelis, V. M.; Kozlitin, E. A. *Radiochemistry* **2009**, *51*, 298–300.
- (30) Tsuruoka, S.; Fugetsu, B.; Khoerunnisa, F.; Minami, D.; Takeuchi, K.; Fujishige, M.; Hayashi, T.; Kim, Y. A.; Park, K. C.; Asai, M.; Kaneko, K.; Endo, M. *Mater. Express* **2013**, *3*, 21–29.